Solid Earth Discuss., 7, 2243–2282, 2015
www.solid-earth-discuss.net/7/2243/2015/
doi:10.5194/sed-7-2243-2015

Solid Earth Discussions
Open Access

Qualitative and quantitative changes in detrital reservoir rocks caused by CO_2-brine-rock interactions during first injection phases (Utrillas sandstones, Northern Spain)

E. Berrezueta[1], **B. Ordóñez-Casado**[1], **and L. Quintana**[1,2]

[1]Instituto Geológico y Minero de España, Oviedo, Spain
[2]Departamento de Geología, Universidad de Oviedo, Oviedo, Spain

Received: 30 June 2015 – Accepted: 21 July 2015 – Published: 11 August 2015

Correspondence to: E. Berrezueta (e.berrezueta@igme.es)

Published by Copernicus Publications on behalf of the European Geosciences Union.

Abstract

The aim of this article is to describe and interpret qualitative and quantitative changes at rock matrix scale of Lower-Upper Cretaceous sandstones exposed to supercritical (SC) CO_2 and brine. The effects of experimental injection of SC CO_2 during the first injection phases were studied at rock matrix scale, in a potential deep sedimentary reservoir in Northern Spain (Utrillas unit, at the base of the Cenozoic Duero Basin).

Experimental wet CO_2 injection was performed in a reactor chamber under realistic conditions of deep saline formations ($P \approx 78$ bar, $T \approx 38\,^{\circ}$C and 24 h exposure time). After the experiment, exposed and non-exposed equivalent sample sets were compared with the aim of assessing possible changes due to the effect of the CO_2-brine exposure. Optical microscopy (OpM) and scanning electron microscopy (SEM) aided by optical image analysis (OIA) were used to compare the rock samples and get qualitative and quantitative information about mineralogy, texture and porous network distribution. Chemical analyses were performed to refine the mineralogical information and to obtain whole rock geochemical data. Brine composition was also analysed before and after the experiment.

The results indicate an evolution of the pore network (porosity increase ≈ 2 %). Intergranular quartz matrix detachment and partial removal from the rock sample (due to CO_2 input/release dragging) are the main processes that may explain the porosity increase. Primary mineralogy (≈ 95 % quartz) and rock texture (heterogeneous sand with interconnected framework of micro-channels) are important factors that seem to enhance textural/mineralogical changes in this heterogeneous system. The whole rock and brine chemical analyses after interaction with SC CO_2-brine do not present important changes in the mineralogical, porosity and chemical configuration of the rock with respect to initial conditions, ruling out relevant precipitation or dissolution at these early stages.

These results, simulating the CO_2 injection near the injection well during the first phases (24 h) indicate that, in this environment where CO_2 displaces the brine, the

SED

7, 2243–2282, 2015

mixture principally generates local mineralogical/textural re-adjustments due to physical detachment of quartz grains.

Consequences deriving from these changes are variable. Possible porosity and permeability increases could facilitate further CO_2 injection but textural re-adjustment could also affect the rock physically. However, it is not clear yet what effect the quartz (solid suspension) could provoke in more distant areas of the rock. Quartz could be transported in the fluid flow path and probably accumulated at pore throats.

1 Introduction and objectives

The capture and geological sequestration of CO_2 is one of the technological options currently contemplated to reduce emissions of greenhouse gases into the atmosphere. Deep geological storage in porous rock formations is considered the most appropriate strategy for CO_2 sequestration (Bachu, 2000; Izgec et al., 2008; Benson and Cole, 2008; Gaus, 2010) and injectivity is a key technical and economic issue for carbon capture and storage (CCS) projects (Bacci et al., 2011). The viability of the CO_2 injection depends mainly on the porosity and permeability of reservoir rocks. CO_2 interaction with the host rock, such as dissolution or precipitation of minerals is also important (e.g. Ross et al., 1982; Sayegh et al.; 1990 and Saeedi et al., 2011), as well as mineral trapping (Kaszuba et al., 2003; Rosenbauer et al., 2005; Liu et al., 2013). Dissolution of supercritical (SC) CO_2 into brine will control the rate of dissolution and precipitation of minerals constituting the porous rock. Volume changes of the solid phase will modify the pore structure, affecting both porosity and permeability of the porous media (André et al., 2007).

CO_2-water-rock interaction experiments represent a useful method to understand and explore the mechanisms and processes of geological storage (Ketzer et al., 2009) and to design safe underground CO_2 storage operations. Bertier et al. (2006) built an experimental setup to evaluate the effect of CO_2-water-rock interactions in three sandstone aquifers concluding that "CO_2-water-rock interactions might significantly in-

SED
7, 2243–2282, 2015

fluence geological sequestration of CO_2". Most of the experimental and theoretical studies are designed to simulate the injection of CO_2, mixed with brine, into rocks at $P-T$ conditions of deep storage environments. The result of many of these experiments was an increase in the porosity/permeability of the reservoir rock caused by partial dissolution of the carbonate components (mainly calcite) (Perkins and Gunter, 1995; Svec and Grigg, 2001; Rochelle et al., 2004; Egermann et al., 2005; Izgec et al., 2005; Gunter et al., 2004; Luquot and Gouze, 2009 and Desbois et al., 2011). However, other set of experiments has shown porosity decreases due to the initial dissolution of carbonates followed by secondary precipitation/mineralisation (Kaszuba et al., 2003; Cailly et al., 2005; Kaszuba et al., 2005; Mito et al., 2008; Sterpenich et al., 2009; Luquot and Gouze, 2009). André et al. (2007) presented numerical modelling of chemical fluid-rock interactions at the SC-CO_2-liquid interface during CO_2 injection into a carbonate reservoir (Paris Basin, France). In this case, two CO_2 injection scenarios were evaluated: CO_2-saturated water injection and pure supercritical CO_2 injection. In these two scenarios, different geochemical processes occurred as the distance from the injection well increased (in the first scenario there was a porosity increase of up to 90%; while, in the second scenario porosity increased about 6 % in most of the reservoir and it decreased in the vicinity of the injection point). Besides, different regions were identified depending on the saturation ranges of liquid and gas phases, associated geochemical conditions and porosity variations during the injection and according to the distance from the injection well (Fig. 1a).

Other investigations focus on the CO_2 injection into potential reservoir rock formations under dry conditions (Kaszuba et al., 2003; Vickerd et al., 2006 and Berrezueta et al., 2013). The injection environment is mainly envisaged as injecting CO_2 mixed with brine into sandstones. However, in near-well conditions, the supercritical CO_2 laterally displaces the brine and occupies the pore space of the rocks, in either dry or near-dry conditions (André et al., 2007; Burton et al., 2008; Luquot and Gouze, 2009; Gaus, 2010). Therefore, dry CO_2 interaction with the storage rock is a realistic scenario that takes place during the initial injection stages. Some theoretical studies (Gaus et

SED
7, 2243–2282, 2015

al., 2008 and Gaus, 2010) and experimental results (Stepernich et al., 2009) on dry CO_2-rock interactions indicate the absence of reactions and consequently negligible textural-mineralogical changes. This is explained by the lack of H_2O in the system that prevents dissolution/precipitation and any kind of chemical reactions. However, experimental studies on dry-CO_2 injection into undersaturated sandstones with high clay matrix content (Berrezueta et al., 2013) concluded in an increase of rock porosity, causing a textural change. This was explained by detachment and partial removal of the intergranular clay matrix from the sandstone samples due to supercritical CO_2 input/release dragging and changes in electrical-polarity forces.

Our research is focussed on experimental injection of supercritical CO_2 into the selected rocks (sandstones saturated by and covered with brine), similarly to previous works e.g. Wdowin et al. (2014) and Tarkowski et al. (2015). We chose the Utrillas sandstones for the present study due to their importance as potential CO_2 reservoirs in Spain. The lithological characteristics of the Utrillas sandstones and the structural features of the area offer favourable conditions for the study of CO_2 storage (García Lobón et al., 2010 and Martínez et al., 2013).

The selected $P-T$ conditions and run-times of our experiments aim to reproduce the reservoir rock dry-wet environment, adjacent to a theoretical injection borehole, (Fig. 1a and b), specifically, at the interface between the supercritical CO_2 bubble and the aqueous solution. This interface acts as an exchange zone where CO_2 diffuses constantly (e.g. Zone 4 defined by André et al., 2007). The experimental $P-T$ conditions were selected to guarantee that the CO_2 was over its supercritical point (Holloway, 1997; Bachu, 2000; Lake, 1989; Span and Wagner, 1996).

Furthermore, the textural-mineralogical and petrophysical changes in the rock samples are studied before and after the experimental injection of supercritical CO_2 for a short period of time (24 h). Special care was put into the development of a model to explain the observed changes. Optical image analysis (OIA) techniques were used to monitor these changes.

SED
7, 2243–2282, 2015

2 Samples: geological setting

The studied samples belong to the unit commonly known as Utrillas sandstones and locally defined as Voznuevo Formation (Evers, 1967) of Upper Albian-Lower Cenomanian age (Lower-Upper Cretaceous transition). The sampling took place in North Spain, at the boundary between the Alpine Cantabrian Mountains and the Cenozoic Duero Basin (Fig. 2a). The Utrillas sandstones belong to a 1100 m thick Cretaceous sequence and crop out near Boñar village in North León province. This Cretaceous sequence lays unconformably on the Paleozoic basement of the Variscan Cantabrian Zone. On top of the Cretaceous sequence, a succession of almost 2500 m thick Cenozoic materials was deposited in the Duero Basin (Fig. 2d). The Cretaceous sequence has been divided into three parts (Manjón Rubio et al., 1982a): (1) a lower detritical part, which corresponds to the Utrillas sandstones, of continental origin; (2) an intermediate or transitional part of Turonian-Santonian age; and (3) an upper carbonate part with limestones and marls of Santonian-Campanian age and marine origin (Fig. 2c). This Cretaceous sequence was deposited in a post-rift stage, at the end of the Cretaceous extensional phase that affected North Spain and produced the opening of the Bay of Biscay (e.g. Gallastegui, 2000).

The Utrillas sandstones, in the study area, are composed of detrital, poorly consolidated or unconsolidated whitish materials ranging from sandstone to conglomerate, with a maximum size of pebbles of 6 cm. The succession is fining upwards with dominating conglomerates at the base and progressively increasing sandstone ratio. The pebbles and grains are mainly of quartzite origin and of subrounded to subangular form, with a sandy and kaolinitic matrix. Argillaceous levels, paleochannels and cross-stratification are frequent and lignites appear locally. This succession was formed in a fluvial braided environment and with a source area composed of acid, mainly granitic and metamorphic, rocks. The transformation from feldspar to kaolin occurred after the deposition and was the result of meteorization processes (Manjón Rubio et al., 1982a).

SED
7, 2243–2282, 2015

The fluvial environment, in which the Utrillas sandstones were formed, represents the proximal part of the Upper Cretaceous North-Iberian paleomargin. Towards the north, this fluvial facies changed into deltaic facies, then talus facies and, finally, deep basin turbiditic facies (Olive Davó et al., 1989). This paleomargin was deformed during the collision between Iberia and Eurasia in Cenozoic times. This compressional event produced the uplift of the Cantabrian Mountains in North Spain and the development of the Duero foreland basin in the frontal part or the range (Alonso et al., 1996). The structure of the sampling area is relatively simple and is characterized by a great monoclinal (Fig. 2d), the formation of which has been related with a south-directed basement thrust inclined to the north (Alonso et al., 1996). In detail the structure is more complex because the inclined limb of the monocline is disrupted by an important fault, known as the Sabero Fault (Sabero-Gordón line of Rupke, 1965), that produces the duplication of the Cretaceous sequence (Fig. 2b and d).

The Utrillas sandstone was sampled in three places of the complex inclined limb of the monocline, in the area of Devesa of Boñar, performing a thorough study of the structure of these target rocks and their seals (Fig. 2b, d and e). The sampling areas "Devesa 1" and "Devesa 2" are located south of the Sabero Fault, in an outcrop of Cretaceous succession dipping 80° towards the south. The sampling area "Devesa 3" is located north of the Sabero Fault in an outcrop dipping 45° also southwards (Fig. 2b and d). For this study, we chose the more consolidated sandstones, located in "Devesa 1", to guarantee the effectiveness of the analysis. The unconsolidated sandstones of Devesa 2 and 3 were discarded for the study. The samples were divided into adjoining and numbered sets of blocks. Each couple of adjoining blocks was used for the experimental test and for the studies before and after CO_2 injection.

SED
7, 2243–2282, 2015

3 Methodology and experimental procedure

3.1 Experimental setup and procedure

The experimental setup employed in this experiment (Fig. 1b) is based on similar systems described by Luquot and Gouze (2009), Luquot et al. (2012), Berrezueta et al. (2013) and Wdowin et al. (2014). However, some modifications were made due to the distinct characteristics of the target rock system. Sample material (rock type and representative sample size), geological environment (pressure, temperature and salinity) and technical equipment (materials for camera, software, pumps, etc.) were all considered for the final arrangement of the experimental device and run conditions. The experiment consists of the exposure of sandstones to SC CO_2 in a reactor with pressure and temperature control. *P*/*T* conditions (78 bar and 38 °C, respectively) were selected to surpass the CO_2 supercritical point (Lake, 1989; Span and Wagner, 1996) and to simulate basic conditions of injection and storage of CO_2 (Holloway, 1997; Bachu, 2000). These conditions are representative of a depth of approx. 800 m. The selected exposure time (24 h) is meant to model the first stage of injection.

The system (Fig. 1b) has two CO_2 cylinders (standard commercial CO_2 at 45 bars) that are linked to the other elements of the system by steel connectors (diameter: 5 mm). The second CO_2 cylinder is connected to a piston pump that operates with a flow of 0.01 g s^{-1}. When the required pressure (78 bar) decreases (due to possible leaks), this pump will inject CO_2 to keep the pressure within the desired values. The piston pump needs a CO_2 initial pressure of 10 bars in order to inject CO_2 into the Hastelloy steel chamber (3000 cm^3), thereby, the pressure between the piston pump and the second CO_2 cylinder has to be decreased by a pressure manometer from 45 to 10 bar. The inside of the chamber is coated with polytetrafluoroethylene (PTFE) to protect the material against corrosion. At the bottom of the chamber, a calorimeter controls the internal temperature. The calorimeter and the pump are linked to the chamber with pressure and temperature sensors and are connected to a computer.

SED
7, 2243–2282, 2015

The experiments began with the saturation of rock samples (6 cubes of 27 cm^3 of each sandstone sample) with natural brine. 600 cm^3 brine was chemically stabilized with the samples for the saturation. 300 cm^3 of this brine was extracted and analysed before SC CO_2 injection. Then, the rock samples were introduced into the chamber together with the rest of brine. The experimental runs comprised: (a) a pressurized CO_2 injection (3 h); (b) a pressurized stabilization (24 h, no CO_2 flow inside the chamber) and (c) CO_2 pressure release (3 h). The CO_2 injection was performed using a constrained hyperbaric chamber-reactor where the dry CO_2 was pumped at pressures and temperatures of 78 bar and 38 °C, respectively. The times of filling and emptying the chamber with supercritical CO_2 were the same (3 h). This is the time required to reach the target pressure and temperature values, from the initial ambient conditions. The same time was used to get back to the ambient conditions at the end of the experimental test. The applied software, HEL 5.1, allows the remote control of the system (experimental conditions) through the development of specific macros (pressure, temperature, time) in real time. All the experimental runs were carried out in the laboratories of the Geological Survey of Spain (IGME) in Tres Cantos, Madrid.

3.2 Methodology of study

The aim of the study was to quantify the possible textural and porosity changes due to experimental CO_2 injection. We began with a detailed petrographic study using optical microscopy (OpM) to identify the major mineral and textural features. The characterization was performed in neighbouring areas of the blocks by OpM (30 µm thin sections) and scanning electron microscopy (SEM, rock samples). Although the thin sections and SEM samples do not exactly correspond to the same sample surface, they are located very close (a few mm) in the original source-sample. The aim of the detailed OpM study and quantification of mineralogical and textural variability was to verify that any changes observed in the experiments were due to the effects of CO_2 effect and not to possible original heterogeneity. Furthermore, chemical analysis of the brine and

SED
7, 2243–2282, 2015

whole rock before and after SC CO_2 injection were performed, as well as microscopic studies of the residue that remained in the reactor chamber after the experiment.

Simultaneously, a detailed study of the configuration of porous system was conducted by combining observation by scanning electron microscopy with backscattered electrons (SEM) and optical image analysis (OIA). This method allows the study of pore size distribution and other porosity parameters (shape, specific surface of pore, etc.). Later, the same procedure was followed for the study of the SC CO_2 exposed rocks. The OIA technique makes it possible to identify, characterize and quantify mineral elements in images captured digitally (Fig. 3) before and after SC CO_2-brine exposure. The general procedure for the automated image analysis was developed adapting the procedures and algorithms described by Berrezueta et al. (2015), in order to quantify the textural and porosity changes (area, roughness of minerals/pore boundaries, fractal dimension, roundness of minerals/pores and porosity) provoked by experimental CO_2 injection. Assessment of pore-network distribution by optical transmitted light studies of thin sections requires distinction between mineral and pore networks according to their optical characteristics. The segmentation of the porous system was made by regions, applying the "thresholding" segmentation method (based on threshold values to turn a raw image into a binary one, the pixels being partitioned according to their intensity value). In this way, we can quantify the evolution of small changes in the configuration of pore network. This work was carried out in the Oviedo IGME laboratory using a Leica DM 6000 polarization microscope and an Image Pro Plus-7.0 software and ProgRes digital camera for pore network study by OIA. SEM studies were performed using a Hitachi TM3000 microscope with X-ray microanalysis equipment.

Additionally, rock samples were analysed by X-ray fluorescence (XRF) and X-ray diffraction (XRD), and brine composition was determined by several methods (ion chromatography, ICP, pH, conductivity measurements). The studies were developed in the facilities of IGME laboratory-Tres Cantos and Oviedo University Laboratory.

SED
7, 2243–2282, 2015

4 Results

4.1 Mineralogical and petrographic characterization and OIA pore-network quantification

4.1.1 Samples before SC CO_2 injection

The studied rock is a medium to very coarse-grained sandstone (grain size from 90–1600 µm, with a mode of 250 µm) with areas of fine to medium grain sizes, showing unoriented and slightly to highly variable porous structure. The pores, that are 80–500 µm (up to 1400 µm) in size, constitute up to 8 to 15 % of the rock volume, although there are special areas with porosity up to 20 %. The grains are from moderately to poorly sorted. There are zones with a slight anisotropy defined by the presence of matrix rich bands. The grain skeleton (Fig. 4a, c and e) consists of quartz (> 95 %), very minor potassium feldspars (orthoclase) and a small amount of micas (muscovite and chlorite). Accessory minerals (a total of 1–5 %) are opaque minerals, such as iron oxides and hydroxides (hematite and limonite), in the form of aggregates of 40–100 µm in size, dispersed in the matrix or as cement. Other accessory minerals are brown and green tourmalines and zircon. The rock is mainly grain supported with a small proportion of matrix (< 5 %) composed mostly by quartz and minor phyllosilicates of the mica and clay groups (muscovite and/or illite and/or kaolinite) and opaque minerals. Locally, cement is present as a film coating iron oxides and sintaxial quartz. According to the Folk (1974) and Pettijohn et al. (1987) classification, it is a quartz-arenite (> 95 % of quartz). Some areas have higher matrix concentration (> 15 %) classified as fine-medium grained quartz-greywacke. The quartz grains are mostly monocrystalline with important size variability. The grains have angular to subangular shapes, from high to low sphericity and with sizes ranging from 90 to 1400 µm. Moreover very rounded grains of polycrystalline quartz (fairly minor amount) appear sometimes with a Fe oxide coating. They are of significant size (900–1900 µm). Grains with internal crystals of > 30 µm size are the most common. On the other hand, there are some polycrystalline

SED
7, 2243–2282, 2015

quartz grains with elongated shapes and large dimensions up to 2800 µm. Sometimes the internal crystalline units of the polycrystalline quartz grains show preferred orientations (meta-quartzite origin). The internal units can be of sizes < 30 µm (chert) or up to 180–240 µm. The orthoclase feldspars are very scarce, have rounded edges with sizes up to 1400 µm and show a significant degree of alteration to iron oxides, phyllosilicates (illite and/or kaolinite) and chlorite.

The porous system reaches estimated visual proportions of 8 to 15 %. Adapting Choquette and Pray (1970) and Lucia (1999) porosity nomenclatures for carbonates, various pore types were identified. "Vuggy" pore type, corresponding to highly spherical and rounded pores with sizes around 50–90 µm are common. "Intercrystalline" type pores were also observed. These are irregularly shaped around skeletal grains with very rounded edges, possibly a product of matrix solution. They present elongated shapes and sizes ranging from 140–220 up to 300 µm. There are also incipient "cavernous" type pores, with elongated shapes, of sizes of ca. 80–170, even 550 µm. In addition, there are "fracture" type pores. The sizes of these pores generally reach 80–200 µm but there are some larger elongated caverns (ca. 1400 µm). "Protected" porosity below some quartz grains (500 µm) was also observed. The mineralogical and pore network distribution has been corroborated by SEM observation (Fig. 5a, c, and e).

The pore network quantification by OIA (Table 1) was carried out in three thin sections with images acquired with a magnification of 10×. The porosity percentage estimated by this method ranges from 6.49 to 18.18 % with an average of 11.41 ± 0.14 %. The maximum and minimum area of pore were 172 100 andt 9.2 µm^2, respectively. The average pore area size was 168 µm^2. Curves of relative and absolute distribution of number of pores versus pore area ranges and diagrams of weighted area related to pore area classes are presented in Fig. 6a and c for the samples before SC CO_2 injection.

SED
7, 2243–2282, 2015

4.1.2 Samples after SC CO_2 injection

The studied rock is a medium to very coarse grained, poorly-sorted sandstone (particle size from 300 to 1800 µm). It is slightly to highly porous with a porosity of 12 to 18 % of the rock volume and with pore size up to 2.5 mm. The grains vary from high to low spherical and from subrounded to rounded shapes and it is noteworthy that the quartz grains have a high degree of fracturing. The rock has scarce anisotropy, primarily defined by a band of higher matrix concentration and opaque minerals (Fe oxides). The skeleton (Fig. 4b, d and f) consists mostly of quartz grains (> 95 %), scarce potassium feldspars (orthoclase) and small amounts of mica (muscovite). Quartz grains show high degree of fracturing and are primarily monocrystalline with high or low sphericity and rounded edges. Their sizes vary from 300 to 1800 µm. Sometimes they are of low sphericity with rounded edges or subangular shapes, with sizes ranging from 240 to 1000 µm, even up to 2.4 mm. On the other hand, polycrystalline quartz is present with internal crystal units < 30 µm, with elongated shapes, rounded edges and grain sizes between 700–1400 µm. Other polycrystalline quartz grains are rounded with sizes up to 1000–2400 µm with internal structural units > 30 µm. Orthoclase feldspars are very rounded and quite spherical, with sizes up to 2.4 mm. They sometimes show alteration containing Fe oxides and phyllosilicates (possibly illite and/or kaolinite). Accessory minerals are opaque minerals (iron oxides associated to iron hydroxides). These opaque minerals appear in the form of large grains surrounding the skeleton grains or as smaller crystals scattered in the sandy-clay matrix or oriented at the edges of matrix rich bands. Other accessory minerals are tourmaline and zircon. The matrix (< 15 %) is composed mainly by quartz and a small amount of phyllosilicates (possibly illite and/ or kaolinite and/or smectite) and iron oxides. Opaque minerals are Fe oxides and hydroxides (hematite and limonite) that are often associated with phyllosilicates (kaolinite and/or illite and/or smectite) and mica (possibly muscovite). Based on the modal content of quartz, feldspars, lithoclasts and matrix content the rock is classified

SED
7, 2243–2282, 2015

as quartz-arenite and some areas with higher matrix content (ca. 15 %) as medium grained quartz-wacke (Folk, 1974; Pettijohn et al., 1987).

The identified porosity is more abundant than in the samples before CO_2 injection. The estimated visual percentage ranges from 12 to 18 %. Adapting Choquette and Pray (1970) and Lucía (1999) nomenclatures, there are various pore types present in the rock. Intercrystalline pores between quartz grains with variable sizes (90–240 µm) were observed. The presence of pores that are arranged in micro-fractures within quartz grains is also common. Cavern type pores appear frequently, with irregular shapes and sizes varying from 700 to 1700 up to 2900 µm. Sometimes they are interconnected by micro-channels. Caverns are generally larger than in the sample before CO_2 injection. Sometimes, matrix rich bands show elongated channel pores following the anisotropy with a maximum dimension of 4.8 mm. The SEM studies (Fig. 5b, d, and f) showed again intergranular spaces constituted by cavern pores interconnected by micro-channels and pore spaces sometimes filled with minerals. Furthermore, the high degree of fracturing leads to fracture type pore development.

The pore network quantification by OIA was developed, as previously described, on digital images acquired using objective lens of 10×. The estimated porosity percentage ranges from 7.06 to 22.05 % (Table 1), with an average of 13.42±0.17 %. The maximum area of pore was 250 000 µm^2 and the minimum was 9 µm^2. The average pore area size was 278 µm^2. Curves of relative and absolute distribution of number of pores versus pore area ranges and diagrams of weighted area related to pore area classes are presented in Fig. 6b and d for the samples after SC CO_2 injection.

4.2 Chemical analysis

The composition of the brine was analyzed before and after the 24 h testing and the results are shown in Table 2. The data of brine composition before and after experimental CO_2 injection show that there were some changes in the chemistry (higher that the total uncertainty of the technique: ≈ 10 %): a decrease (ca. 30 %) of the Ca^{2+}, Mg^{2+} and SO_4^{2-} contents and an increase on the HCO_3^- and NO_3^- contents. Other chemical

SED
7, 2243–2282, 2015

parameters also decreased as a result of the CO_2 injection: the pH changed from 7.2 to 5.27 and the conductivity also decreased around 12 %.

Total rock analyses were performed on blocks with and without experimental CO_2-brine exposure. The values and uncertainties are presented in Table 3. There were changes in the following contents: increase of MgO (30 %), Na_2O (20 %) and CaO (ca. 200 %). We considered as significant a change over the uncertainties given by the laboratory for each element, which uncertainty values range from 6.8 to 19.9 % depending on the element. Two samples were analysed by XRD, one previous to brine exposure and to SC CO_2 injection and the other after the SC CO_2-brine experiment. These analyses only detected quartz, the other phases being present in quantities below the detection limit of this technique. Furthermore, the residue that remained in the chamber of the reactor after the experiment, was studied (Fig. 7). This residue consisted mainly of quartz in two different fractions: a fine fraction with sizes around 20 µm and another fraction with rounded quartz grains sometimes reaching 1 mm in size.

5 Discussion

In the studied Utrillas sandstones, OpM and SEM techniques allowed us to detect qualitative changes in the pore network in the samples before and after SC CO_2 injection. Compared to the pre-experiment samples, we can point out that, in general, after the experiment larger pores are more common (700–1800 µm) and cavern type pores and channels dominate (Figs. 4a–b and 5a–b). There is also an increase of grain fracturing (Fig. 4c and d; Fig. 5c and d). Moreover, the edges of quartz grains before the experiment contain angular pits (Fig. 5e), while pits in quartz after the experiment are less numerous and distinctly rounded and enlarged (Fig. 5f).

Quantification of these changes were systematically carried out applying OIA (Fig. 3). This study reveals an increase of porosity (Δn) of 0.57–1.58–3.87 % with an average of 2.01 % (Table 1), which value is higher than the uncertainty of the OIA tech-

SED
7, 2243–2282, 2015

nique (≈ 1.25 %) (Demirmen, 1972; Grove and Jerram, 2011). The lower error of this method as compared to others is one of the advantages of the OIA technique (e.g. error of point counting is around 2.5 %; Chayes and Faibain, 1951; Grove and Jerram, 2011).

The OIA technique also allowed us a complete characterization of the pore network through curves of relative and absolute distribution of the number of pores versus pore area ranges (Fig. 6) and diagrams of weighted area related to pore area classes for samples before and after SC CO_2 injection. The pore area ranges measured by OIA are between 9 and 250,000 μm^2. The distribution of data shows that ≈ 99 % of pores correspond to pores smaller than 1250 μm^2 (Fig. 6a). In the CO_2 injected sample (Fig. 6b) these small pores represent ≈ 98 % of all the pores. The diagrams of the weighted area related to pore area classes before (Fig. 6c) and after SC CO_2 injection (Fig. 6d) show that the contribution of the first class of pore area is ca. 35 % of the total porosity for pre-experiment samples and ca. 25 % of the total porosity for samples after the experiment. The approximate contributions of cumulative weighted pore area for the main percentiles for the sample before SC CO_2 injection are: < 1250 μm^2 (25 %), 7500 μm^2 (50 %), and 38 750 μm^2 (75 %). On the other hand, the sample after injection shows contributions of 25 % of pore area of 1250 μm^2, 50 % of 8750 μm^2, and 75 % of 65 000 μm^2. In general, in the original samples there are more pores of smaller and intermediate pore area classes than in the ones after the injection. Besides, the maximum sizes of pore area are larger in the injected samples.

The brine chemistry study showed that Na^+, K^+, Cl^- and SiO_2 values did not suffer any relevant changes after the injection. On the other hand, the Ca^{2+}, Mg^{2+} and SO_4^{2-} content decreased by approx. 30 % (Table 2), probably all as a result of local mineral precipitation of Mg, Ca and Na minerals, evidenced by an increase of these oxides in the chemistry of the rock after the experiment (Table 3). The brine chemistry data, in relative terms is similar to those found in the literature (Kaszuba et al., 2005), but different to the analysis completed by Wdowin et al. (2014), Luquot et al. (2012); Yu et al. (2012). This is probably due to the initial composition of our samples, conditioned by

SED
7, 2243–2282, 2015

the chemically resistant quartz (95 % wt) and the short period of our experimentation (24 h). We can say that preliminarily CO_2-brine contact with the rock initiated some mineral precipitation though not to a relevant scale. It also caused brine pH reduction (changing from 7.2 to 5.2), similarly to other cases (Kaszuba et al., 2005). The pH reduction is due to the increase of carbonic acid and NO_3^- content of the brine after the experiment (Table 2). The higher amount of carbonic acid originates from the CO_2 dissolution in the brine, while that of the NO_3^- may be due to reactions with organic material present in the rock sample. The overall data of the total rock composition of before and after SC CO_2-brine exposure do not show precipitation/dissolution of mineral phases. We can conclude that that the reactions between minerals and fluids were not significant (Gunter et al., 1997 and Hitchon, 1996) and the changes in the porosity configuration (Table 1) are due to physical processes.

The observed and measured changes in the studied samples are due to the SC CO_2-brine exposure and can be of importance in the vicinity of the injection well (Fig. 1a) where the interaction of the CO_2 and the rock takes place initially in wet conditions (Kharaka et al., 2006; Gaus, 2010; André et al., 2007). Any modification in mineralogy and porosity (Figs. 4, 5 and Table 1) changing the rock texture could affect the injection well and its closest environment and hence the injection efficiency (Wdowin et al., 2014). Our experimental investigation indicates that the main effects observed after the experiment are relevant to the pore network characteristics and quantification, while changes regarding chemical characteristics of the brine and total rock are minor.

All these considerations allow us to build a conceptual model for the experimental SC CO_2 injection (Fig. 8a to d). The CO_2 input and release affected the quartz matrix and quartz skeletal grains in different ways that finally lead to detachment and partial re-adjustment of the quartz volume (except in the area with firmly fixed quartz grains or areas without CO_2-brine access). These effects resulted in a partial loss of the quartz (both grains and matrix), present as residue after the experiment (Fig. 7). Our conceptual model consists of four stages.

SED
7, 2243–2282, 2015

- Stage 1 (Fig. 8a): Initial mineralogical and textural conditions of the rock saturated with brine. Quartz constitutes 95 % of the rock sample and brine partially fills intergranular spaces.
- Stage 2 (Fig. 8b): pressurized SC CO_2 injection: initial CO_2 input would mix with brine and percolate through the rock pore system generating a mechanical dragging force probably opening/widening some of the inter quartz-particle cracks.
- Stage 3 (Fig. 8c): pressurized CO_2-brine stabilization: this stage extends through most of the experimental run (24 h). During this time, SC CO_2 continues to diffuse into the pore structure causing accommodation inside (small fractures) and between quartz grains, producing instability in the rock cohesion.
- Stage 4 (Fig. 8d): CO_2-brine pressure release and expansion: Intra-quartz particle CO_2 expansion during pressure release would promote further internal quartz breakdown and generation of free micro-quartz grains (Fig. 4b, d and f; Fig. 5b, d and f). This pressure release and gas and brine expansion generated outward dragging forces that probably favoured partial loss of quartz grains that were collected in the chamber when the experiment was finished. This would allow us to explain the porosity increase in the rock.

This model explains how the indirect mineralogical-compositional changes, (identified by OpM, SEM Figs. 4 and 5), may be related to possible de-cohesion of the quartz matrix possibly caused by CO_2-brine pressure (Fauria and Rempel, 2011; Berrezueta et al., 2013). If the system is open, the de-cohesion causes part of the mineral phases of the matrix to leave the system generating a mineralogical-compositional change. The nature of this change is physical and not chemical. The possible de-cohesion of the matrix, by the action of CO_2, leads logically to an increase in the porosity. Therefore, the observed increase in porosity is most probably caused by this de-cohesion and matrix loss, in our experiments.

SED
7, 2243–2282, 2015

6 Conclusions

Quantitative assessment of petrography and mineralogy by OIA can be an important tool for geosciences, providing numerical values as a key to the successful interpretation of the rock texture and mineralogy.

The proposed methodology, consisting of mineralogical and petrographic studies by OpM, SEM and OIA techniques on sandstones subjected to SC CO_2-brine exposure (78 bar, 38 °C, during 24 h), proved to be highly effective for the identification and measurement of changes in the pore network. For this study, the Utrillas sandstones were selected due to their potential as CO_2 reservoir in Spain. However, the same methodology could be applicable for future studies considering other rock types, different CO_2 storage conditions or longer periods of exposure time.

The influence of the original rock composition and texture is very important and leads to different effects of the SC CO_2-brine exposure. The study of potential changes at rock matrix scale depends on the facies variations of any sedimentary formation, when evaluating a possible CO_2 reservoir. The facies studied in this work is characterized by 95 % quartz content and heterogeneous rock texture, where micro-channels in the quartz matrix areas favour the SC CO_2-brine injection resulting in the development of bigger cavities and pore channels. The main pore evolution measured by OIA was an increase of porosity (2.10 %) and a readjustment of pore network distribution regarding pore size classes.

The chemical analysis of whole rock and brine, before and after SC CO_2-brine injection, point out the prevalence of physical processes with regard to chemical processes (dissolution/precipitation) during the early injection phases. The chemical-compositional evolution of the analysed elements did not evidence significant mineralogical processes. Supercritical CO_2 causes brine pH to decrease as a consequence of carbonic acid increase, validating published models about the effect of supercritical CO_2 on brine.

SED
7, 2243–2282, 2015

The results of this experiment show that the changes occurred due to physical process and may have an important impact on the behaviour of reservoir rocks during first injection phases of SC CO_2: (i) changes in the rock system that lead to the porosity evolution could facilitate further CO_2 injection, (ii) mobilization of solid material (quartz) should be considered during experiments and/or future modelling of the reservoir.

Acknowledgements. The authors would like to thank the funding provided through the ALGECO2-IRMC Project (Instituto Geológico y Minero de España: 2294-2013), CO2-Pore Project (Plan Nacional de España: 2009-10934, FEDER-UE), Minería XXI Project (CYTED: 310RT0402) and DIA-CO2 Projects I and II (CIUDEN: ALM/09/032 and ALM/12/028). Thanks are due to Roberto Martínez, Félix Mateos, Luís González-Menéndez, Isabel Suárez and Ricardo Molinero for providing help in OIA techniques, SEM analysis, data acquisition, and statistical treatment for rock sample collection and to Timea Kovacs for her suggestions.

References

Alonso, J. L., Pulgar, J. A., García-Ramos, J. C., and Barba, P.: Tertiary basins and Alpine tectonics in the Cantabrian Mountains (NW Spain), in: Tertiary basins of Spain: The stratigraphic record of crustal Kinematics, edited by: Friend, P. F. and Dabrio, C. J., Cambridge University Press, Cambridge, 214–227, 1996.

André, L., Audigane, P., Azaroual, M., and Menjoz, A.: Numerical modelling of fluid-rock chemical interactions at the supercritical CO_2-liquid interface during CO_2 injection into a carbonate reservoir, the Dogger aquifer (Paris Basin, France), Energ. Convers. Manage., 48, 1782–1797, 2007.

Bacci, G., Korre, A., and Durucan, S.: An experimental and numerical investigation into the impact of dissolution/precipitation mechanisms on CO_2 injectivity in the wellbore and far field regions, Int. J. Greenh. Gas Con., 5, 579–588, 2011.

Bachu, S.: Sequestration of CO_2 in geological media: criteria and approach for site selection in response to climate change, Energ. Convers. Manage., 41, 953–970, 2000.

Benson, S. M. and Cole, D. R.: CO_2 sequestration in deep sedimentary formations, Elements, 4, 325–331, 2008.

SED
7, 2243–2282, 2015

Berrezueta, E., González-Menéndez, L., Breitner, D., and Luquot, L.: Pore system changes during experimental CO_2 injection into detritic rocks: Studies of potential storage rocks from some sedimentary basins of Spain, Int. J. Greenh. Gas Con., 17, 411–422, 2013.
Berrezueta, E., González-Menéndez, L., Ordoñez-Casado, B., and Olaya, P.: Pore network quantification of sandstones under experimental CO_2 injection using Image Analysis, Computer and Geosciences, 77, 97–110, 2015.
Bertier, P., Swennen, R., Laenen, B., Lagrou, D., and Dreesen, R.: Experimental identification of CO_2-water-rock interactions caused by sequestration of CO_2 in Westphalian and Buntsandstein sandstones of the Campine Basin (NE-Belgium), J. Geochem. Explor., 89, 10–14, 2006.
Burton, M., Kumar, K., and Bryant, S. L.: Time-dependent injectivity during CO_2 storage in aquifers, in: Symposium on Improved Oil Recovery Tulsa, Okla. Proceedings: Richardson, Tex., Society of Petroleum Engineers, paper SPE 113937, p. 15, 2008.
Cailly, B., Le Thiez, P., Egermann, P., Audibert, A., Vidal-Gilbert, S., and Longaygue, X.: Geological storage of CO_2: A state-of-the-art of injection processes and technologies, Oil Gas Sci. Technol., 60, 517–525, 2005.
Chayes, F. and Fairbairn, H. W.: A test of the precision of thin-section analysis by point counter, Am. Mineral., 36, 704–712, 1951.
Choquette, P. W. and Pray, L. C.: Geologic nomenclature and classification of porosity in sedimentary carbonates, AAPG Bull., 54, 207–250, 1970.
Demirmen, F.: Operator error in petrographic point-count analysis: a theoretical approach, J. Int. Ass. Math. Geol., 4, 35–43, 1972.
Desbois, G., Urai, J. L., Kukla, P. A., Konstanty, J., and Baerle, C.: High-resolution 3D fabric and porosity model in a tight gas sandstone reservoir: a new approach to investigate microstructures from mm-to nm-scale combining argon beam cross-sectioning and SEM imaging, J. Petrol. Sci. Eng., 78, 243–257, 2011.
Egermann, P., Bazin, B., and Vizika, O.: An experimental investigation of reaction-transport phenomena during CO_2 injection, in: SPE Middle East Oil and Gas Show and Conference, Society of Petroleum Engineers, 2005.
Evers, H. J.: Geology of the Leonies between the Bernesga and Porma rivers, Cantabrian Mountains, NW Spain, Leidse Geol. Meded., 41, 83–151, 1967.
Fauria, K. E. and Rempel, A. W.: Gas invasion into water-saturated, unconsolidated porous media: Implications for gas hydrate reservoirs, Earth Planet. Sc. Lett., 312, 188–193, 2011.

SED
7, 2243–2282, 2015

Folk, R. L.: Petrology of Sedimentary Rocks. Hemphill's, Austin, Texas, 170 pp., 1974.
Gallastegui, J.: Estructura cortical de la Cordillera y Margen Continental Cantábricos: Perfiles ESCI-N, Trabajos de Geología, Universidad de Oviedo, 22, 9–234, 2000.
García Lobón, J. L., Reguera García, M. I, Martín León, J., Rey Moral, C., and Berrezueta, E.: Plan de selección y caracterización de áreas y estructuras favorables para el almacenamiento geológico de CO_2 en España, Resumen ejecutivo Instituto Geológico y Minero de España (IGME), Madrid, 2010.
Gaus, I.: Role and impact of CO_2-rock interactions during CO_2 storage in sedimentary rocks. Int. J. Greenh. Gas Con., 4, 73–89, 2010.
Gaus, I., Audigane, P., Andre, L., Lions, J., Jacquement, N., Durst, P., Czernichowski, I., and Azaroual, M.: Geochemical and solute transport modelling for CO_2 storage, what to expect from it?, Int. J. Greenh. Gas Con., 2, 605–625, 2008.
Grove, C. and Jerram, D. A.: jPOR: An ImageJ macro to quantify total optical porosity from blue-stained thin sections, Comput. Geosci., 37, 1850–1859, 2011.
Gunter, W. D., Wiwehar, B., and Perkins, E. H.: Aquifer disposal of CO_2-rich greenhouse gases: extension of the time scale of experiment for CO_2-sequestering reactions by geochemical modelling, Miner. Petrol., 59, 121–140, 1997.
Gunter, W. D., Bachu, S., and Benson, S.: The role of hydrogeological and geochemical trapping in sedimentary basins for secure geological storage of carbon dioxide. Geological Society, London, Special Publications, 233, 129–145, 2004.
HEL user's guide (5.1) for Windows: WinISO Software control System Reactor, 2009.
Hitchon, B.: Aquifer disposal of carbon dioxide: hydrodynamic and mineral trapping-proof of concept, Geoscience Publishing Ltd, Alberta, Canada, 165 pp., 1996.
Holloway, S.: An overview of the underground disposal of carbon dioxide, Energ. Convers. Manage., 38, S193–S198, 1997.
IMAGE-PRO® R PLUS user's guide (7.0) for Windows: Software Program of Media Cybernetics. Inc., 2009.
Izgec, O., Demiral, B., Bertin, H. J., and Akin, S.: Experimental and numerical investigation of carbon sequestration in saline aquifers, in: SPE/EPA/DOE Exploration and Production Environmental Conference, Society of Petroleum Engineers, 2005.
Izgec, O., Demiral, B., Bertin, H. J., and Akin, S.: CO_2 injection into saline carbonate aquifer formations I: laboratory investigation, Transport Porous Med., 72, 1–24, 2008.

SED
7, 2243–2282, 2015

Kharaka, Y. K., Cole, D. R., Hovorka, S. D., Gunter, W. D., Knauss, K. G., and Freifeld, B. M.: Gas-water-rock interactions in Frio Formation following CO_2 injection: Implications for the storage of greenhouse gases in sedimentary basins, Geology, 34, 577–580, 2006.

Kaszuba, J. P., Janecky, D. R., and Snow, M. G.: Carbon dioxide reaction processes in a model brine aquifer at 200 °C and 200 bars: implications for geologic sequestration of carbon, Appl. Geochem., 18, 1065–1080, 2003.

Kaszuba, J. P., Janecky, D. R., and Snow, M. G.: Experimental evaluation of mixed fluid reactions between supercritical carbon dioxide and NaCl brine: Relevance to the integrity of a geologic carbon repository, Chem. Geol., 217, 277–293, 2005.

Ketzer, J. M., Iglesias, R., Einloft, S., Dullius, J., Ligabue, R., and De Lima, V.: Water-rock-CO_2 interactions in saline aquifers aimed for carbon dioxide storage: experimental and numerical modeling studies of the Rio Bonito Formation (Permian), southern Brazil, Appl. Geochem., 24, 760–767, 2009.

Lake, L. W.: Enhanced oil recovery, Pentice Hall, Englewood Cliffs, NJ, 1989.

Liu, H., Hou, M. Z., Gou, Y., and Were, P.: Simulation of CO_2-Water-Rock Interaction Processes-Mineral Scaling Problems in Saline Formations, in: Clean energy systems in the subsurface: production, storage and conversion, Springer Series in Geomechanics and Geoengineering, 233–248, 2013.

Lobato, L., García-Alcalde, J. L., Sánchez de Posada, L. C., Truyols, J., and Servicio Geológico, S. A. H. V. L. (Cuenca Ciñera-Matallana): Mapa geológico de España a E, 1 : 50.000, núm. 104 "Boñar", Segunda Serie, Primera Edición, Instituto Geológico y Minero de España (IGME), Madrid, 1985.

Lucia, F. J.: Carbonate reservoir characterization: Berlin, Springer-Verlag, 226 pp., 1999.

Luquot, L. and Gouze, P.: Experimental determination of porosity and permeability changes induced by injection of CO_2 into carbonate rocks, Chem. Geol., 265, 148–159, 2009.

Luquot, L., Andreani, M., Gouze, P., and Camps, P.: CO_2 percolation experiment through chlorite/zeolite-rich sandstone (Pretty Hill Formation-Otway Basin-Australia), Chem. Geol., 294, 75–88, 2012.

Manjón Rubio, M., Vargas Alonso, I., Colmenero Navarro, J. R., García-Ramos, J. C., Gutiérrez Elorza, M., and Molina, E.: Memoria del Mapa geológico de España E. 1:50.000, Hoja núm. 130 (Vegas del Condado), Segunda Serie, Primera Edición, Instituto Geológico y Minero de España (IGME), Madrid, 1982a.

SED
7, 2243–2282, 2015

Manjón Rubio, M., Vargas Alonso, I., Colmenero Navarro, J. R., García-Ramos, J. C., Crespo Zamorano, A., and Matas González, J.: Mapa geológico de España E. 1:50.000, Hoja núm. 130 (Vegas del Condado), Segunda Serie, Primera Edición, Instituto Geológico y Minero de España (IGME), Madrid, 1982b.

Martínez, R., Suarez, I., Carneiro, J., Zarhloule, Y., Le Nindre, Y., and Boavida, D.: Storage capacity evaluation for development of CO_2 infrastructure in the west Mediterranean, Energy Procedia, 37, 5209–5219, 2013.

Mito, S., Xue, Z., and Ohsumi, T.: Case study of geochemical reactions at the Nagaoka CO_2 injection site, Japan, Int. J. Greenh. Gas Con., 2, 309–318, 2008.

Olivé Davó, A., Álvaro López, M., Ramírez del Pozo, J., and Aguilar Tomás, M.: Memoria del Mapa Geológico de España a Escala 1 : 200.000, Hojas No 5/12 (Bermeo/Bilbao), Instituto Tecnológico Geominero de España, Madrid, 208 pp., 1989.

Perkins, E. H. and Gunter, W. D.: Aquifer disposal of CO_2-rich greenhouse gasses: modelling of water-rock reaction paths in a siliciclastic aquifer, in: Water-rock Interactions, edited by: Kharaka, Y. K. and Chidaev, O. V., Brookfield, Rotterdam, 895–898, 1995.

Pettijohn, F. J., Potter, P. E., and Siever, R.: Sand and Sandstones, Springer, Berlin, 553 pp., 1987.

Quintana, L., Pulgar, J. A., and Alonso, J. L.: Displacement transfer from borders to interior of a plate: a crustal transect of Iberia, Tectonophysics, accepted, 2015.

Rochelle, C. A., Czernichowski-Lauriol, I., and Milodowski, A. E.: The impact of chemical reactions on CO_2 storage in geological formations: a brief review, Geological Society, London, Special Publications, 233, 87–106, 2004.

Rosenbauer, R. J., Koksalan, T., and Palandri, J. L.: Experimental investigation of CO_2-brine-rock interactions at elevated temperature and pressure: implications for CO_2 sequestration in deep-saline aquifers, Fuel Process. Technol., 86, 1581–1597, 2005.

Ross, G. D., Todd, A. C., Tweedie, J. A., and Will, A. G.: The Dissolution Effects of CO_2-Brine Systems on the Permeability of UK and North Sea Calcareous Sandstones, in: SPE/DOE 10685 Enhanced Oil Recovery Symposium, Society of Petroleum Engineers, 1982.

Rupke, J.: The Esla Nappe, Cantabrian Mountains (Spain), Leidse Geol. Meded., 32, 1–74, 34 fig., 6 láms, Leiden, 1965.

Saeedi, A., Rezaee, R., Evans, B., and Clennell, B.: Multiphase flow behaviour during CO_2 geo-sequestration: Emphasis on the effect of cyclic CO_2-brine flooding, J. Petrol. Sci. Eng., 79, 65–85, 2011.

SED
7, 2243–2282, 2015

Sayegh, S. G., Krause, F. F., Girard, M., and DeBree, C.: Rock/fluid interactions of carbonated brines in a sandstone reservoir: Pembina Cardium, Alberta, Canada, SPE Formation Evaluation, 5, 399–405, 1990.

Span, R. and Wagner, W.: A new equation of state for carbon dioxide covering the fluid region from the triple-point temperature to 1100 K at pressures up to 800 MPa, J. Phys. Chem. Ref. Data, 25, 1509–1596, 1996.

Sterpenich, J., Sausse, J., Pironon, J., Géhin, A., Hubert, G., Perfetti, E., and Grgic, D.: Experimental ageing of oolitic limestones under CO_2 storage conditions: Petrographical and chemical evidence, Chem. Geol., 265, 99–112, 2009.

Svec, R. K. and Grigg, R. B.: Physical effects of WAG fluids on carbonate core plugs, in: SPE 71496 Annual Technical Conference and Exhibition, Society of Petroleum Engineers, 2001.

Tarkowski, R., Wdowin, M., and Manecki, M.: Petrophysical examination of CO_2-brine-rock interactions-results of the first stage of long-term experiments in the potential Zaosie Anticline reservoir (central Poland) for CO_2 storage, Environ. Monit. Assess., 187, 1–10, 2015.

Trujols, J., Álvarez, F., Arbizu, M.-A., García-Alcalde, J. L., García-López, S., Martínez-Chacón, M. L., Méndez Bedia, I., Méndez-Fernández, C. A., Menéndez, J. R., Sánchez de Posada, L., Sotos, F., Lobato, L., and Rodríguez Fernández, L. R.: Memoria del Mapa geológico de España E, 1 : 50.000, Hoja núm. 104 (Boñar), Segunda Serie, Primera Edición, Instituto Geológico y Minero de España (IGME), Madrid, 1984.

Vickerd, M. A., Thring, R. W., Arocena, J. M., Li, J. B., and Heck, R. J.: Changes in porosity due to acid gas injection as determined by X-ray computed tomography, J. Can. Petrol. Technol., 45, 6 pp., doi:10.2118/06-08-TN1, 2006.

Wdowin, M., Tarkowski, R., and Franus, W.: Determination of changes in the reservoir and cap rocks of the Chabowo Anticline caused by CO_2-brine-rock interactions, Int. J. Coal Geol., 130, 79–88, 2014.

Yu, Z., Liu, L., Yang, S., Yang, S., Li, S., and Yang, T.: An experimental study of CO_2-brine-rock interaction at in situ pressure-temperature reservoir conditions, Chem. Geol., 326–327, 88–101, 2012.

SED
7, 2243–2282, 2015

Table 1. Total porosity of Utrillas sandstones, before and after SC CO_2-brine exposure, measured by Optical Image Analysis (OIA).

	Before SC CO_2-brine		After SC CO_2-brine		Porosity variation		Interpretation
	Porosity %	Average %*	Porosity %	Average %*	Difference %	Total Average %	
Sample 1	18.18	11.41 ± 0.14	22.05	13.42 ± 0.17	3.87	2.01	
Sample 2	9.55		11.13		1.58		Increase
Sample 3	6.49		7.06		0.57		

* Uncertainly (1.25 %) given by Oviedo-IGME Laboratory.

SED
7, 2243–2282, 2015

Table 2. Chemical composition of natural brine before and after the experiment.

	Rock before CO_2 and brine (mg L^{-1})*	Rock after CO_2 and brine (mg L^{-1})*	Interpretation
Na^+	2378 ± 237.80	2351 ± 235.10	No change
K^+	139 ± 13.90	114 ± 11.40	No change
Ca^{2+}	570 ± 57.00	440 ± 44.00	Decrease: 30 % (Δ = 130 mg L^{-1})
Mg^{2+}	268 ± 26.80	200 ± 20.00	Decrease: 34 % (Δ = 68 mg L^{-1})
Cl^-	5200 ± 520	4640 ± 464.00	No change
SO_4^{2-}	624 ± 62.40	464 ± 46.40	Decrease: 34 % (Δ = 160 mg L^{-1})
HCO_3^-	14 ± 1.40	36 ± 3.60	Increase: 157 % (Δ = 22 mg L^{-1})
NO_3^-	1.1 ± 0.11	10 ± 0.10	Increase: 809 % (Δ = 8.9 mg L^{-1})
SiO_2	9.3 ± 0.93	8.3 ± 0.83	No change
pH	7.2 (pH. Unit.)	5.27 (pH. Unit.)	Decrease: 36 % (Δ = 1.93)
Conductivity	15 350 (mS cm^{-1})	13 650 (mS cm^{-1})	Decrease: 20 % (Δ = 1700 mS cm^{-1})

* Uncertainty (10 %) given by Madrid-IGME Laboratory (Water Analysis).

SED
7, 2243–2282, 2015

Table 3. Chemical composition of whole rock (Utrillas sandstone) before and after the experiment. Uncertainty given by IGME Laboratory (XRF Analysis).

	Uncertainty (%)	Rock before CO_2 and brine (%)	Rock after CO_2 and brine (%)	Interpretation
SiO_2	8.20	97.15 ± 2.5260	96.81 ± 2.5430	No change
Al_2O_3	11.57	0.98 ± 0.1135	1.12 ± 0.1300	No change
Fe_2O_3	9.55	0.30 ± 0.0290	0.28 ± 0.0270	No change
MnO	9.31	0	0	No change
MgO	7.96	0.03 ± 0.0025	0.04 ± 0.0030	Increase: 33 % (Δ = 0.01 mg L^{-1})
CaO	6.80	0.04 ± 0.0030	0.12 ± 0.0080	Increase: 200 % (Δ = 0.08 mg L^{-1})
Na_2O	8.20	0.05 ± 0.0040	0.06 ± 0.0050	Increase: 20 % (Δ = 0.01 mg L^{-1})
K_2O	19.94	0.08 ± 0.0160	0.08 ± 0.0160	No change
TiO_2	8.37	0.03 ± 0.0025	0.03 ± 0.0025	No change
P_2O_5	10.95	0.01 ± 0.0010	0.01 ± 0.0010	No change
LOI	12.00	0.48 ± 0.0540	0.64 ± 0.0770	Increase: 33 % (Δ = 0.16 mg L^{-1})
TOTAL		99.16	99.20	

SED
7, 2243–2282, 2015

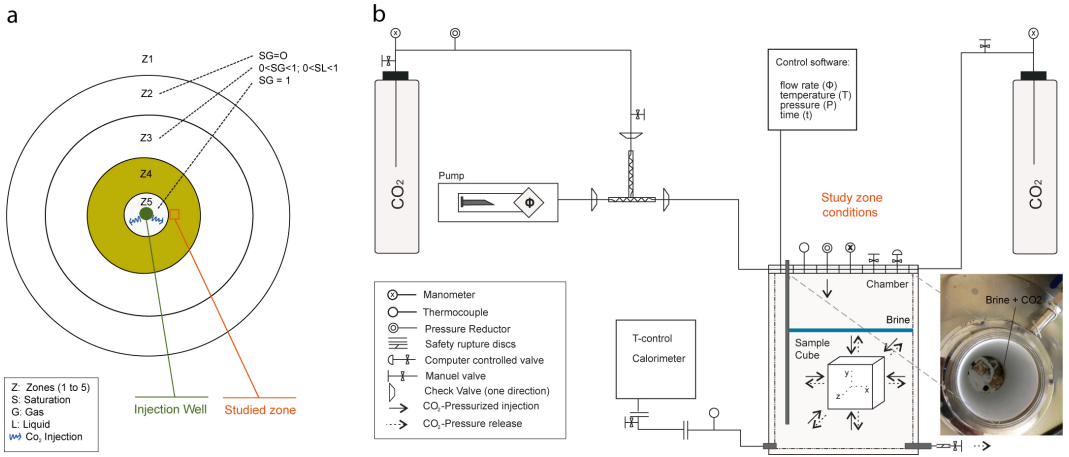

Figure 1. (a) Conceptual diagram of the reactive zones (Z1, Z2, Z3, Z4 and Z5) around the injection well acording to André et al. (2007) and Gaus et al. (2008). Zone 1: Zone not affected by CO_2 injection; Zone 2: Acicified zone with dissolution and precipition of minerals. Zone 3: Dissolution and precipitation of minerals (e.g. calcite and dolomite) and highly buffered pH. Zone 4: Highly saline water and salt precipitation (e.g. NaCl and Ma_2SO_4). Zone 5: Dehydratation reactions in open systems. **(b)** Layout of the experimental setup. Reactor system used for the pressurized CO_2 injection (modified from Berrezueta et al., 2013).

SED
7, 2243–2282, 2015

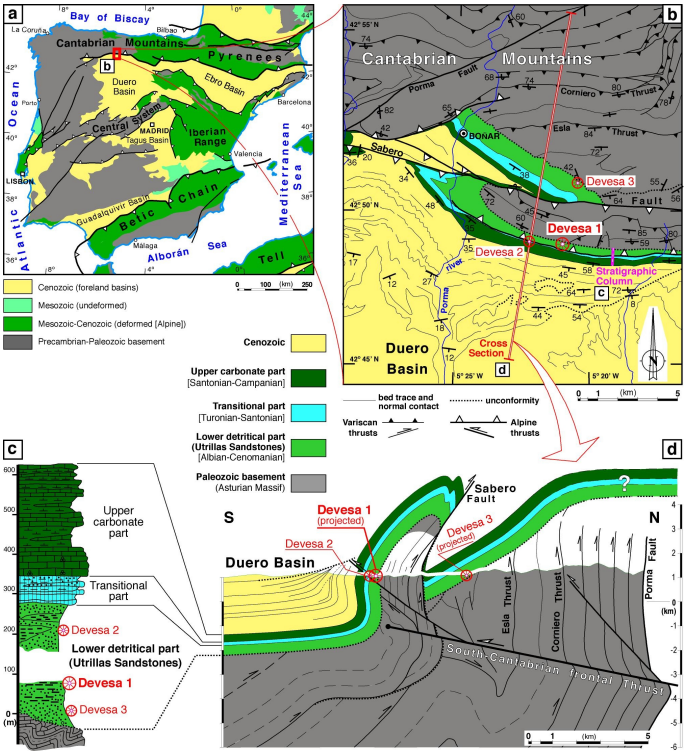

Figure 2. (a) Location of the studied area in North Spain; modified from Quintana et al. (2015) **(b)** Geological map and location of the sampling areas modified from Lobato et al. (1985), Manjón Rubio et al. (1982b) and Alonso et al. (1996). **(c)** Stratigraphic column of the Cretaceous succession of the studied area. Location in "b". Manjón Rubio et al. (1982b). **(d)** Geological cross-section along the sampling areas: boundary between the Cantabrian Mountains and the Duero Basin. The geometry of the South Cantabrian frontal thrust and of the Cenozoic materials of the Duero Basin taken from Alonso et al. (1996). Location in **(b)**.

SED
7, 2243–2282, 2015

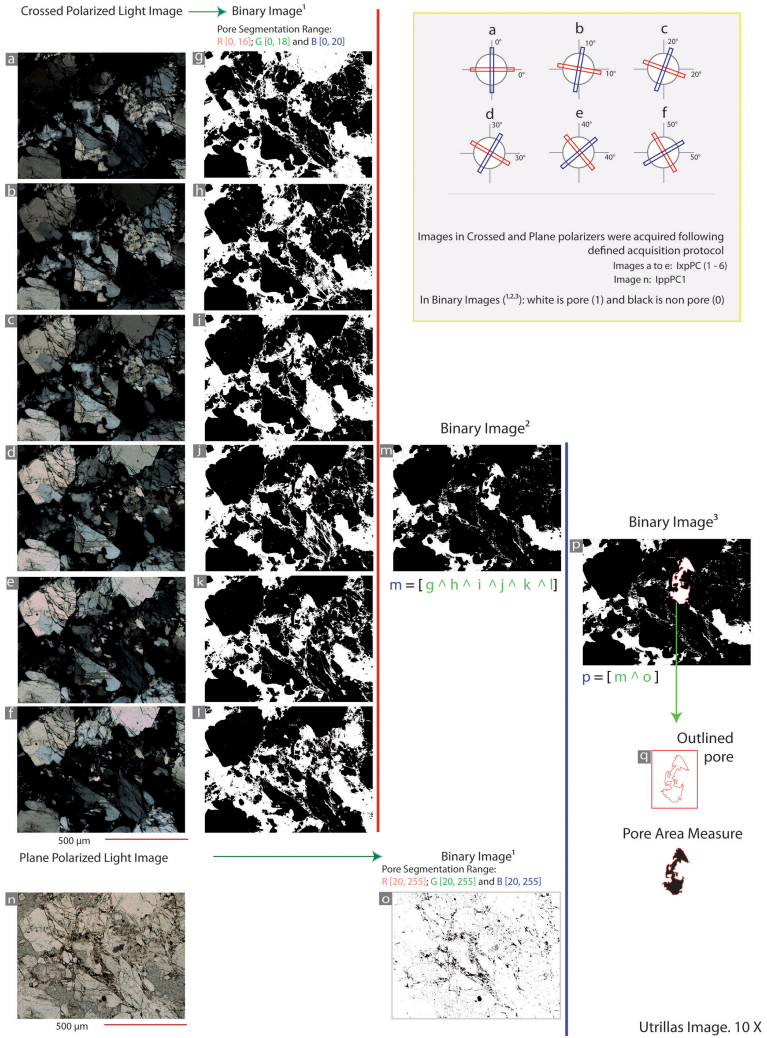

SED
7, 2243–2282, 2015

Changes in detrital reservoir rocks caused by CO_2-brine-rock interactions

E. Berrezueta et al.

Figure 3. Schematic representation of the sequence of pore segmentation and pore area quantification performed on digital images (modified from Berrezueta el al., 2015) of the studied Utrillas sandstone. (**a** to **f**) Images under cross polarized light conditions. (**g** to **l**) Binary images[1] obtained using pore segmentation ranges: R(0–16); G(0–18) and B(0–20). **(m)** Binary image[2] obtained by the interception of binary images[1] (**g** to **l**). **(n)** Image under plane polarized light conditions. **(o)** Binary image[1] obtained using pore segmentation ranges: R(20–255); G(20–255) and B(20–255). **(p)** Binary image[3] obtained by the interception of binary images **(m)** and **(o)**. **(q)** Pore outlined image.

SED
7, 2243–2282, 2015

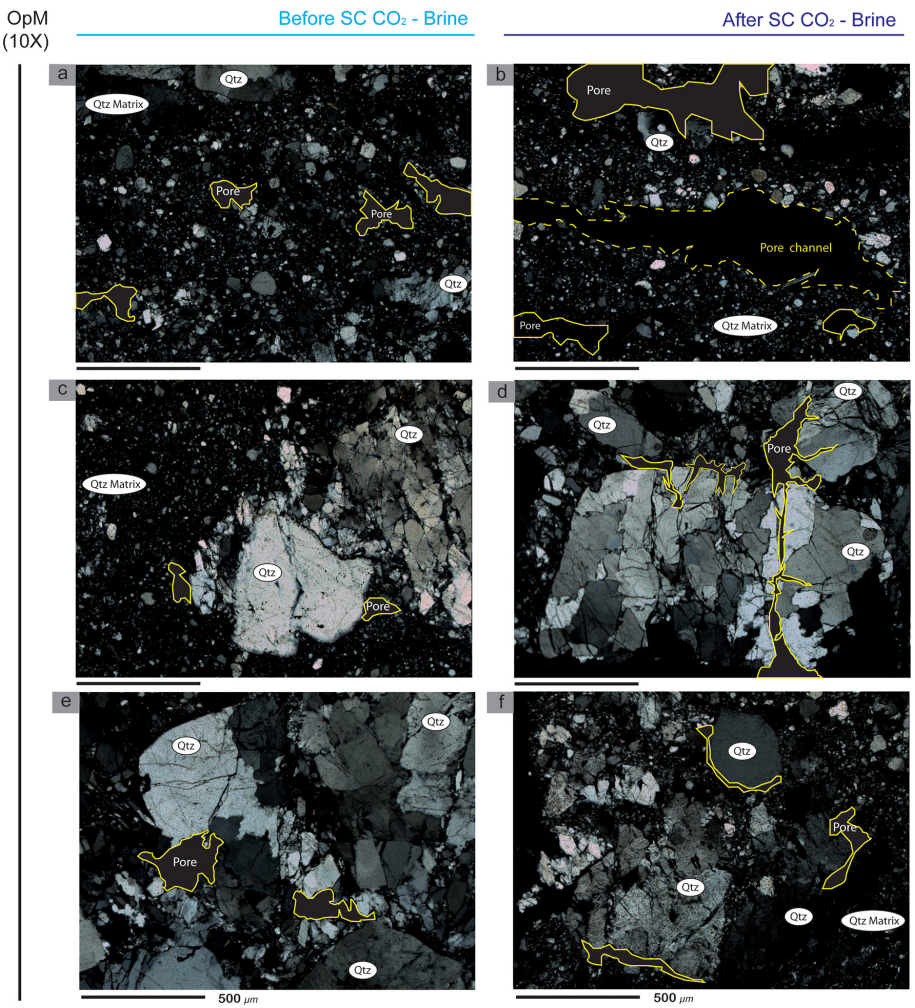

SED
7, 2243–2282, 2015

Changes in detrital reservoir rocks caused by CO_2-brine-rock interactions

E. Berrezueta et al.

Figure 4. Textural and mineralogical characterization of the Utrillas sandstones. Optical microscopy images obtained under cross-polarized light conditions acquired using objective lens of 10×. Left images (**a**, **c** and **e**) correspond to samples before SC CO_2 injection; showing the main textural and mineralogical features corresponding to quartz grains and sandy matrix and intercrystalline pores within the matrix or in the vicinity of skeletal quartz grains. Right images (**b**, **d** and **f**) correspond to samples after SC CO_2 injection; showing no changes in the mineralogical features and a pore network characterized by the presence of channels, caverns and pores within large quartz grains.

SED
7, 2243–2282, 2015

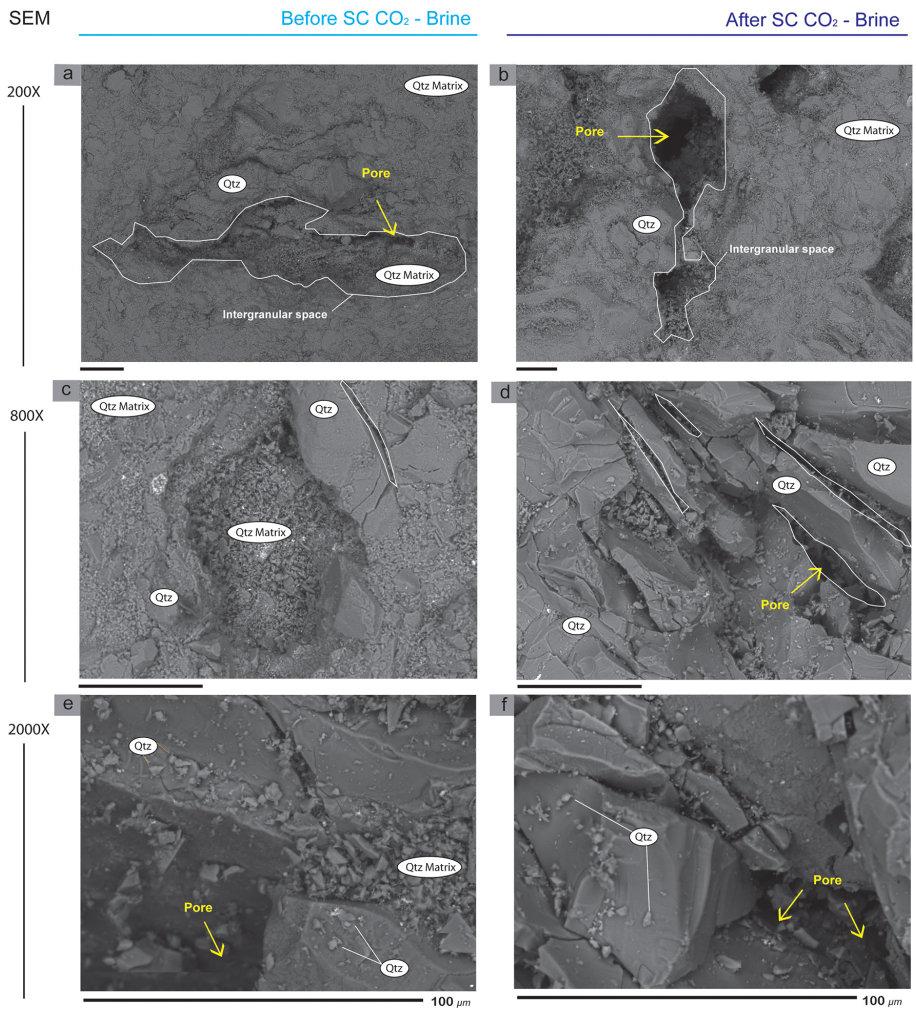

SED
7, 2243–2282, 2015

Changes in detrital reservoir rocks caused by CO_2-brine-rock interactions

E. Berrezueta et al.

Figure 5. Secondary electron SEM micrographs of the Utrillas sandstones. Left images (**a**, **c** and **e**) correspond to samples before SC CO_2 injection. Right images (**b**, **d** and **f**) correspond to samples after SC CO_2 injection. **(a)** Intergranular space filled with minerals; **(b)** intergranular spaces constituted by cavern pores interconnected by micro-channels with pore spaces sometimes filled with minerals; **(c)** intercrystalline space; **(d)** high degree of fracturation of quartz grains; **(e)** the edges of quartz grains in the starting material (before CO_2-brine exposure) contain angular pits; **(f)** pits in quartz from the experiment are less numerous and distinctly rounded and enlarged.

SED
7, 2243–2282, 2015

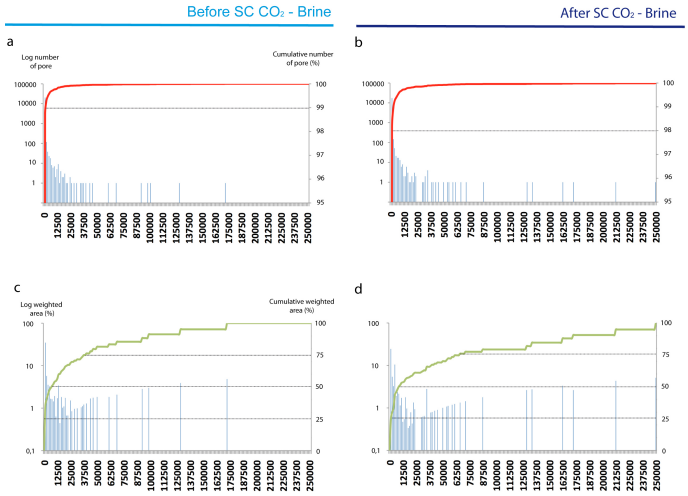

Figure 6. (a) *x* axis vs. left *y* axis: frequency diagrams of number of pores (Log scale) related to pore area classes (μm^2) before CO_2_injection (blue bars). *x* axis vs. right *y* axis: cumulative number of pores (%) related to pore area (μm^2) (red symbols). Red dashed line represents the contribution of the first class of pore area. **(b)** *x* axis vs. left *y* axis: frequency diagrams of weighted pore area (Log scale) related to pore area (μm^2) after CO_2_injection (blue bars). *x* axis vs. right *y* axis: cumulative weighted pore area (%) related to pore area classes (μm^2) (green symbols). Black dashed lines represent percentiles 25, 50, 75. **(c)** *x* axis vs. left *y* axis: frequency diagrams of number of pores (Log scale) related to pore area (μm^2) before CO_2 injection (blue bars). *x* axis vs. right *y* axis: cumulative number of pores (%) related to pore area (μm^2) (red symbols). Red dashed line represents the contribution of the first class to pore area. **(d)** *x* vs. left *y* axis: frequency diagrams of weighted pore area (Log scale) related to pore area (μm^2) after CO_2 injection (blue bars). *x* axis vs. right *y* axis: cumulative weighted pore area (%) related to pore area classes (μm^2) (green symbols). Black dashed lines represent percentiles 25, 50, 75. Minimum pore size considered in the study is $> 9\,\mu m^2$.

SED
7, 2243–2282, 2015

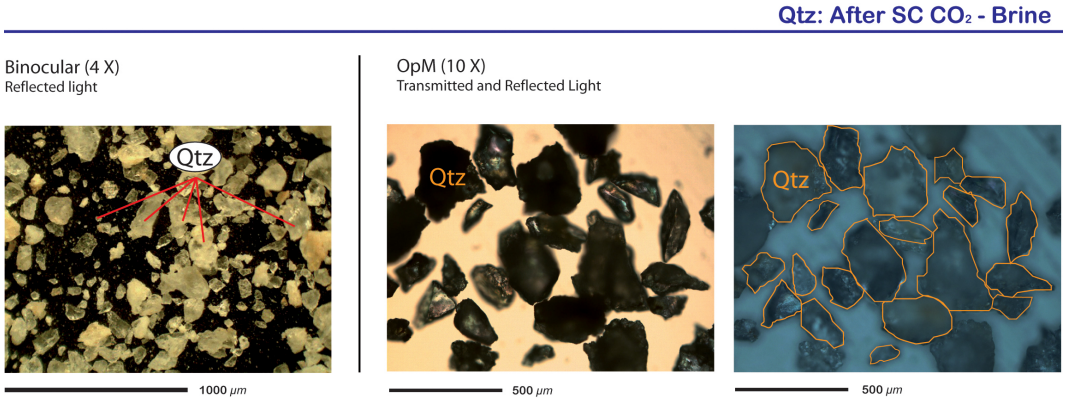

Figure 7. Photomicrographs by binocular microscope (reflected light) and by optical microscope (transmitted and reflected light) of the residue that remained in the reactor chamber after the experiment.

SED
7, 2243–2282, 2015

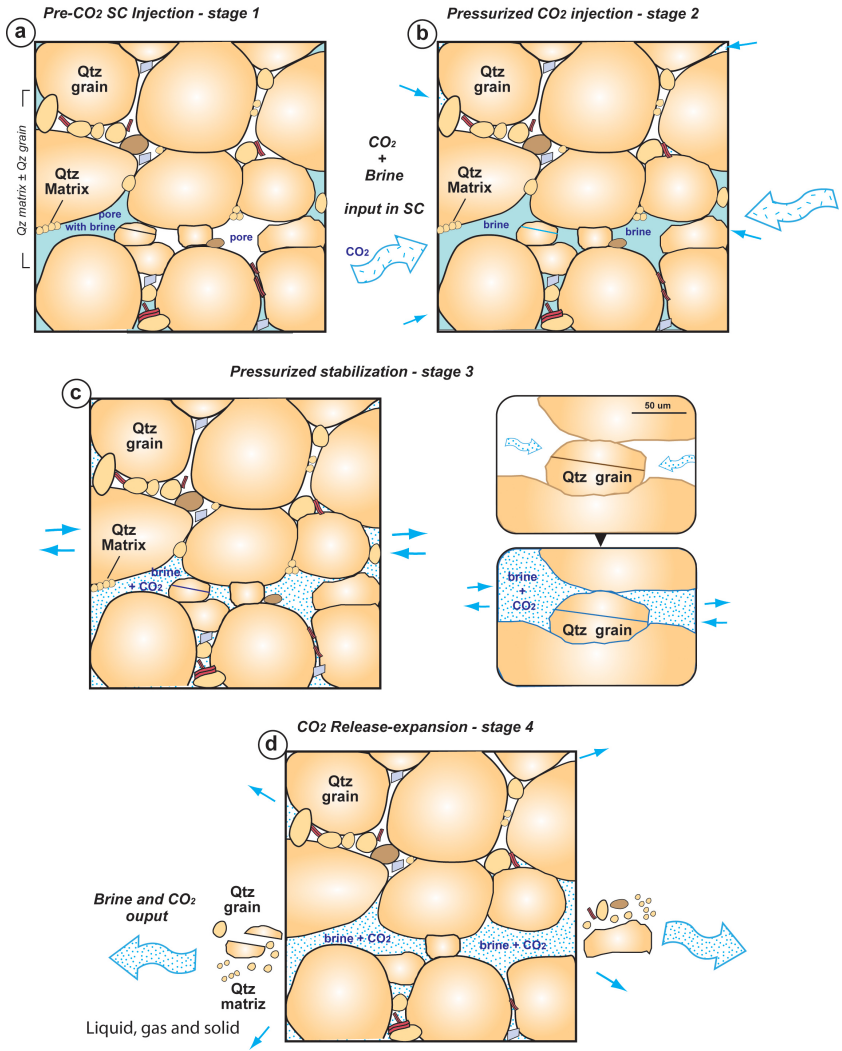

SED
7, 2243–2282, 2015

Changes in detrital reservoir rocks caused by CO_2-brine-rock interactions

E. Berrezueta et al.

Figure 8. Scheme of the model developed from the observed mineralogical/textural changes after the SC CO_2 injection in the Utrillas sandstones. As a summary: **(a)** initial mineralogy and texture of the sandstones: quartz is the 95 % of the rock sample and brine partially fills some intergranular spaces. **(b)** When the pressurized SC CO_2 injection begins, the injected gas fills the pore network (pores filled with brine and empty pores). **(c)** During supercritical experimental stage, the pressurized CO_2 and brine is accommodated inside quartz grains (small fractures) and in the contacts between quartz, producing instability in the original rock cohesion. **(d)** When the pressure releases, at the end stage of the experiment, CO_2 and brine expands generating more instability inside the sample, provoking an outwards drag force that causes leaks and may explain the observed quartz loss in the samples after the experiment.

SED
7, 2243–2282, 2015